

Performance of Porous Carbon as Catalyst Support for Anode from Rice Husk in a Direct Methanol Fuel Cell

Yilhoon Yi^{1,2}, Bong-Do Lee¹, Sang-Kyung Kim^{1,3}, Doo-Hwan Jung^{1,3}, Eun-Mi Jung⁴, Sang-Moon Hwang⁴, Se-Young Choi², Dong-Hyun Peck^{1,3,*}

¹ Fuel Cell Research Center, Korea Institute of Energy Research (KIER), 305-343 Daejeon, Republic of Korea

² Department of Materials Science and Engineering, Yonsei University, 120-749 Seoul, Republic of Korea

³ Major of Advanced Energy Technology, University of Science and Technology (UST), 305-333 Daejeon, Republic of Korea

⁴ Research Institute, Pro-Power Co., 864-2 Dunsan, Bongdong, Wanju, 565-902 Jeollabuk-do, Republic of Korea

*E-mail: dhpeck@kier.re.kr

Received: 23 March 2016 / Accepted: 3 May 2016 / Published: 4 June 2016

This study aims to investigate preparation process of porous carbon as a catalyst support from rice husk (RH) and to measure its electrochemical characteristics for use in a direct methanol fuel cell (DMFC). During heat treatment of RH in inert atmosphere, organic compounds decompose and partly change to H₂O, CO, CO₂, and volatile compounds, remaining carbon and silica. Two types of porous carbon (RH-N₂ and RH-HF) derive from rice husk are used as a catalyst support. RH-N₂ is processed with a heat treatment and carbonization. RH-HF is prepared by etching of RH-N₂ with HF. The samples show a porous structure and high specific surface areas. An anode catalyst is prepared with an impregnation method with RH-N₂ and RH-HF. The catalysts have a superior electrochemical active surface area as measured by the CO stripping and CV methods. Finally, single-cell tests of DMFCs are conducted to analyze the characteristics of the PtRu/C catalyst.

Keywords: porous carbon, rice husk, catalyst support, single cell, direct methanol fuel cell

1. INTRODUCTION

Environmental pollution and energy depletion are critical issues currently faced by humans. Naturally, fuel cells have drawn much attention as an eco-friendly next-generation solution. They are obtained through a reverse electrolysis reaction of water. They are also able to generate electrical energy directly by an electrochemical reaction using oxygen and hydrogen. Direct methanol fuel cell

(DMFC) is considered to be a promising power source for portable devices because of its easy transportation and storage of liquid methanol instead of hydrogen as a fuel. This simplifies the fuel supply system and entire power device.

However, there are several obstacles preventing their commercialization. The greatest problem is finding a feasible catalyst. The amount of Pt has decreased, while its price has increased. This is a major challenge to those companies producing excellent catalyst activators. This has resulted in much research with the goal of finding a novel means for manufacturing non-platinum catalysts [1] and new catalysts.

A conventional catalyst supporter mainly uses numerous porous carbon materials, such as carbon black [1,2], CNTs [3-6], CNFs [7,8], SiO₂ [9] and others. Porous carbon has useful features, such as a controllable specific surface area, the ability to be formed into various structures and shapes, and good electric thermal conductivity. Because it retains excellent properties such as simultaneous chemical resistance, there is great demand for this material.

Rice husk (RH) is a by-product of the agricultural industry. It is usually burned or dumped in fields as waste. Numerous researchers have searched for a solution to this environmental problem by recycling it as an energy resource. RHs usually contain organic compounds such as lignin, cellulose and hemicelluloses, and other inorganic compounds [10]. During heat treatment of RH in inert atmosphere, organic compounds decompose and partly change to H₂O, CO, CO₂, and volatile compounds, remaining carbon and SiO₂ [11]. RH has usually high ash contents in the range of 10~20 wt% compared to other biomass materials. The ash is 87~97 wt% silica [12]. RH is an excellent source of both porous carbon and silica [13]. When the organic compounds decomposed and inorganic compounds in RH are removed, the mesopores are developed. RH carbon is a porous type of carbon with a high porous structure and can be a useful resource in catalysts.

These features have motivated many researchers to investigate RH carbon in a broad range of applications, such as activated carbon [14-16], lithium-ion batteries [17,18], concrete [19] and others. Despite these important porous materials, there have been few papers that dealt with a porous carbon as catalyst support for fuel cells.

This paper tried proposes a novel method for producing a new porous carbon as catalyst support for DMFC with RH, which is an agricultural by-product. To analyze the structure of the porous carbon from RH, nitrogen adsorption-desorption curves were used to calculate the specific surface area and pore volume. And the surface of the porous carbon from RH was examined by means of SEM and FE-TEM. The properties of the catalyst were analyzed through the XRD pattern. Also, cycle voltammetry, anode stripping method, and single-cell test were used for electrochemical analysis of the PtRu/C catalyst. The results show the first attempts to use porous carbon from RH as catalyst support for fuel cells.

2. EXPERIMENTAL

2.1 Preparation of porous carbon

The experiments for porous carbon were prepared and conducted as follows. First, RH from a rice mill (Guryong, Yuseong, Daejeon City, Republic of Korea) was washed with distilled water to

remove impurities. Next, the RH was dried at 110 °C for 24 h in a dryer. A grinding process followed in a grinding machine with 0.2 mm sieve rings (Fritsch, Germany), after which it was processed in a sieve machine (size: <100 μm). As a pretreatment, it was burned at 260 °C for 3 h with dry air (200cc min^{-1}) in a tube furnace (RH-PR). After those processes, it was pyrolyzed and carbonized at 700 °C for 1 h under a nitrogen (>99.999%) atmosphere (200cc min^{-1}) in a tube furnace.

The carbonized material was etched using 2 M of hydrofluoric acid (HF) solution (J. T. Baker Chemicals, USA) for half an hour to remove any silica (RH-HF). Both RH- N_2 and RH-HF were refluxed with 10 wt% hydrochloric acid (HCl) (Junsei Chemical Co, Japan) and 10 wt% sulfuric acid (H_2SO_4) (Junsei Chemical Co, Japan) at 80 °C for 5 h separately to remove impurities and to treat the surfaces. Finally, the porous carbon was washed with pure water until it reached pH 7. The experimental schematic is shown in Fig. 1.

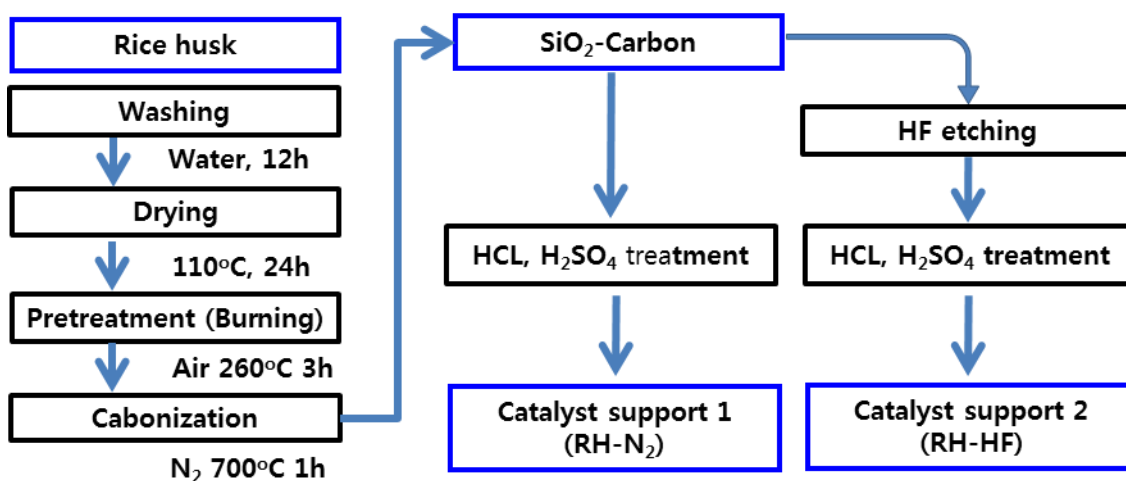


Figure 1. Schematic of the preparation of porous carbon from rice husk.

Vulcan XC-72R (Cabot Co., USA), which is a commercial carbon black powder, was also treated with 10 wt% sulfuric acid.

2.2. Preparation of the PtRu/C catalyst

The catalyst was synthesized with PtRu alloy nanoparticles and RH carbon catalyst support with an impregnation method. The samples (RH- N_2 , RH-HF, XC-72R) were sonicated with deionized water. $\text{H}_2\text{PtCl}_6 \cdot 6\text{H}_2\text{O}$ (Aldrich, USA) and $\text{RuCl}_3 \cdot 3\text{H}_2\text{O}$ (Aldrich, USA) were dissolved in distilled water as precursors of the alloy and stirred for 2 h. Prepared carbon samples and precursors were mixed and stirred for 1 day to prepare the PtRu solution. Approximately 60 wt% of the Pt and Ru metal contents was applied at a molar ratio of Pt and Ru of 1:1. The pH degree of the mixed solution with metal ions was held at 9 by adding an ammonia solution. Each mixed solution of the samples and metal ions was poured into a NaBH_4 solution instantly [20]. After 20 min, the prepared catalysts were filtered, washed with boiling water for 3 h, and dried until they reached pH 7.

2.3. Morphology of porous carbon and PtRu/C

The structure of the porous carbon from RH was examined means of scanning electron microscopy (SEM, Hitachi, S-4700 and S-4800, Japan) using a 5.0 kV emission beam and by FE-TEM (JEM-ARM200F, JEOL, Japan). The catalysts prepared from RH were also analyzed by same FE-TEM. For the SEM analysis, a powdered sample was thoroughly dispersed over a piece of carbon tape stuck onto a copper sample holder. For the FE-TEM analysis, a very small quantity of the sample, which had been finely dispersed in ethanol, was dropped onto a micro-grid. The thermal characteristics were analyzed by a TG device (Netzsch, STA 409 PC, Germany) from 20 °C to 900 °C at a heating rate of 5 °C min⁻¹. The specific surface area and pore structure of the RH were measured with a nitrogen adsorption-desorption isotherm at -196°C using a surface area analyzer (Belsorp Mini, Japan). The specific surface area with V_m -values using the slope and intercept of a BET (Brunauer-Emmett-Teller) plot using the BET equation were calculated. The volume and size of the samples for pores were measured with the BJH (Barrett-Joyner-Halenda) method while applying the Kelvin equation. The sizes of the Pt particles on the catalyst were confirmed in an X-ray diffraction (XRD) analysis using the Scherrer equation. The XRD were done with a Rigaku DMAX-2500 diffractometer using Cu K α radiation. They were scanned at 5.0° min⁻¹ for 2 θ values between 10° and 90°.

2.4. Electrochemical analysis

The catalytic activities and performances of the prepared PtRu catalysts were measured by means of an anode stripping method (CO stripping) and by cyclic voltammetry (CV). An Autolab instrument (PGSTAT204, Metrohm Autolab, Netherlands) was used to drive the electrochemical results. A platinum mesh and an Ag/AgCl electrode were used as the counter electrode and the reference electrode, respectively, for the electrochemical measurements. To activate the electrode catalyst, ink was prepared by the dispersal of PtRu/C catalyst powder in ethanol (Junsei Chemical Co, Japan) with 10wt% of a Nafion solution (DuPont Fluoroproducts, USA). Then, 10 μ l of the catalyst ink was dropped onto a glassy carbon electrode and allowed to dry. For the CO stripping voltammetry, pure CO was added to 0.5M of H₂SO₄ as an electrolyte solution (Junsei Chemical Co, Japan) for 20 min at a fixed potential of 0.05 V (versus Ag/AgCl), after which high-purity (>99.999%). N₂ was bubbled for 30 min to remove the CO dissolved in the electrolyte solution. The current-potential cycles were obtained from -0.2 to 0.8 V (versus Ag/AgCl) at a scan rate of 20 mV s⁻¹ and a temperature 30 °C. For the CV experiment, N₂ gas was purged without a CO supply for nearly 30 min before starting the experiment. The CV tests for H₂-adsorption/desorption were conducted in a 0.5M H₂SO₄ electrolyte. The MOR method for the methanol oxidation reaction was conducted in a 0.5 M H₂SO₄ + 1M CH₃OH electrolyte.

The commercial catalyst of 60 wt% PtRu/C (JM10100, Johnson Matthey, UK) was used as an anode catalyst to compare the performance with RH-N₂ and RH-HF catalysts. 67 wt% Pt/C catalyst (TEC10E70TPM, Tanaka, Japan) was selected as the cathode catalyst. To make the catalyst slurry, a 10 wt% Nafion dispersion solution (DuPont Fluoroproducts, USA), 1-propanolsolution (Junsei Chemical Co, Japan) and 2-propanolsolution (Junsei Chemical Co, Japan) were used. TGP-H-060

(Toray, Japan) with PTFE 5 wt% treated in a laboratory was used as a gas diffusion layer (GDL) for an anode after a hydrophobic treatment with a polytetrafluoroethylene (PTFE) emulsion. 25BC (SGL Carbon, Germany) was used as the GDL on the cathode, which was treated with PTFE. The slurry was brushed onto both sides of the GDLs (9 cm^2) until the Pt loading reached 2 mg cm^{-2} . The electrode layers and a Nafion 115 membrane (DuPont Fluoroproducts, USA) were hot-pressed using a Laboratory Press (Model M, Carver, USA) at $150 \text{ }^\circ\text{C}$ for 1 min at a pressure of 10 MPa to fabricate the MEA. The performance of a single cell was measured with an electrochemical test system (WonA-Tech., Korea) in galvanostatic polarization mode. The performance of the MEA was evaluated from 40°C to 80°C several times. A solution of 1 M of methanol was fed into the anode at a flow rate of 3 ml min^{-1} and air (400 ml min^{-1}) was supplied to the cathode. An electronic load (EL-1010D, Dae-Jin Instrument Co., Korea) was used to evaluate the performance of a single cell.

3. RESULTS AND DISCUSSION

3.1 Characterization of the carbons

Fig. 2 illustrates the nitrogen adsorption-desorption isothermal and mesopore distribution of the raw material (Raw), the pretreated sample (RH-PR), the carbonization sample (RH-N₂) and the etching carbon (RH-HF). The amounts of nitrogen adsorption and desorption grew in the following order: Raw, RH-PR, RH-N₂, and RH-HF. Two samples with RH-N₂ and RH-HF greatly increased after the carbonization process. The same result is shown in graph of the mesopore distribution. The pore structure affects the catalytic activities of the catalyst support. Specifically, mesopores are an important factor for catalyst support. More mesopores imparted the more benefits with regard to performance of the catalysts [1].

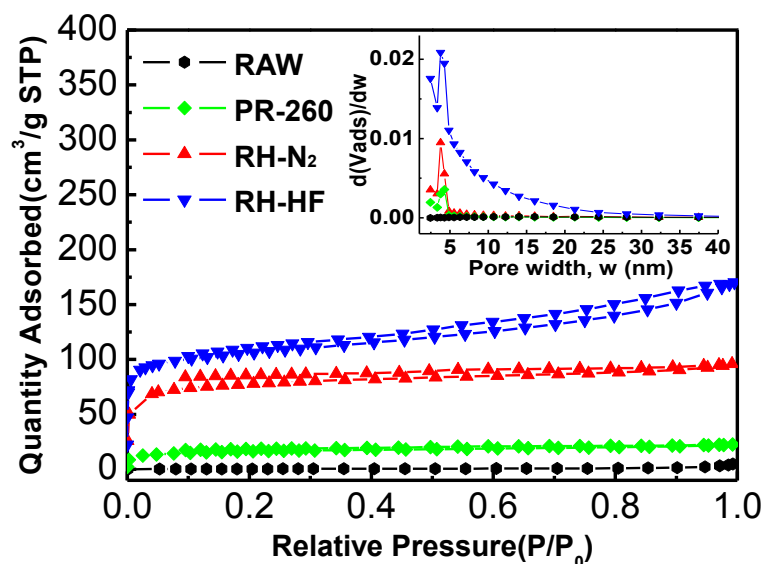


Figure 2. N₂ adsorption isotherms at 77 K and mesopore distribution of the carbon samples: Raw; RH-PR; RH-N₂ and RH-HF.

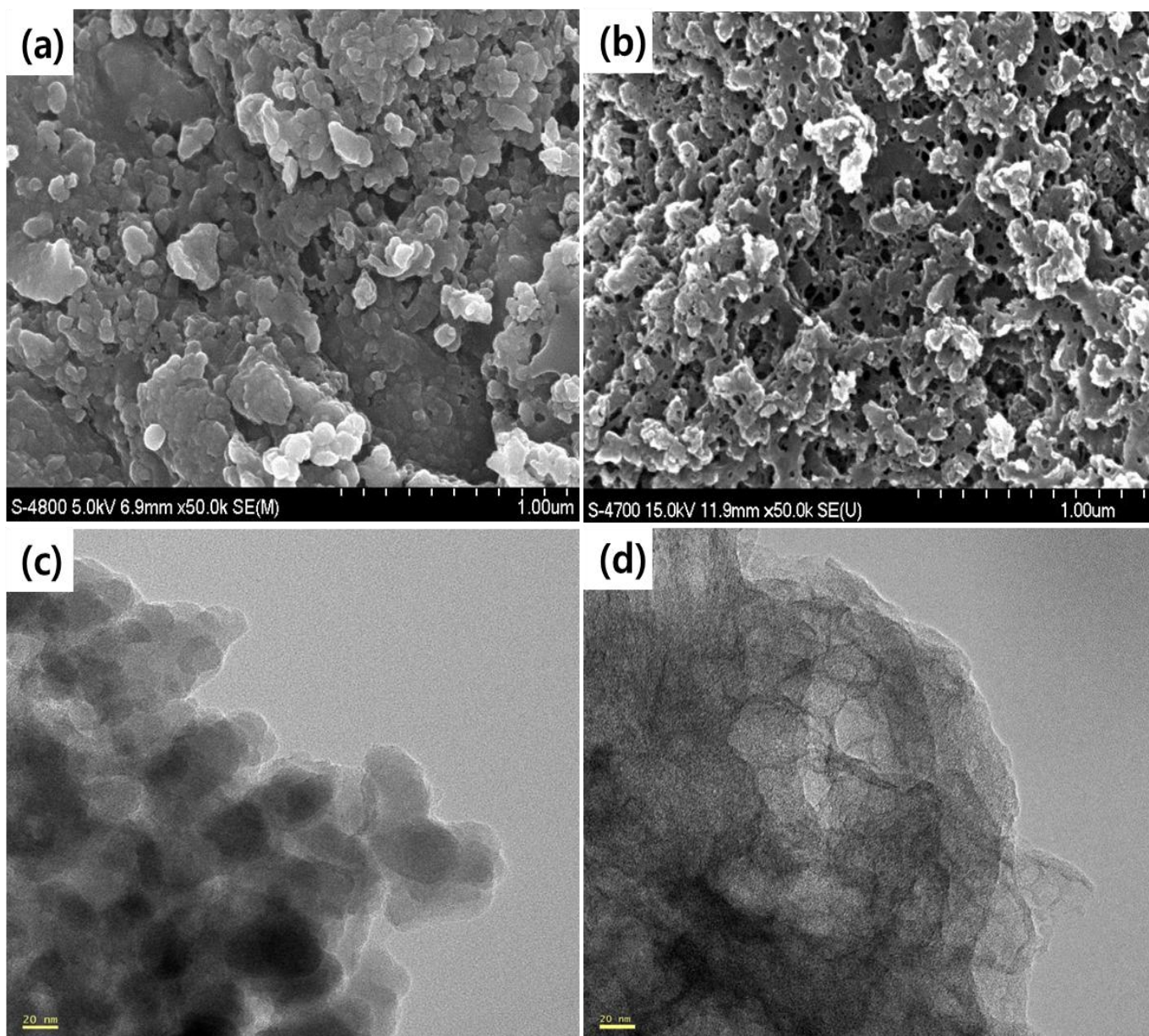


Figure 3. SEM images of porous carbon samples: (a) RH-N₂ and (b) RH-HF, and FE-TEM images of porous carbon samples: (c) RH-N₂ and (d) RH-HF.

The pore size of the RH-HF carbon had a diameter of 2~35 nm after the removal of silica from rice husk by a hydrofluoric acid solution. SEM and FE-TEM were used to distinguish the pore structures of RH-N₂ and RH-HF carbons. In Fig. 3 (a), the surface area of RH-N₂ is dense and packed. Mesopores are rare there. However, it can be confirmed that number of pores with a plurality of sizes formed in the RH-HF carbon, which was etched by a HF solution, as shown in Fig. 3 (b). Additionally, more pores are shown in (d) as compared to (c) in Fig. 3. The RH-HF carbon shows more porous than that of the RH-N₂ carbon.

The amounts of pores and the specific surface area of RH-HF carbon were increased by removing a number of silica present on the surface of carbon. Higher BET surface area and total pore volume of RH-HF carbon can be explained by Fig. 4.

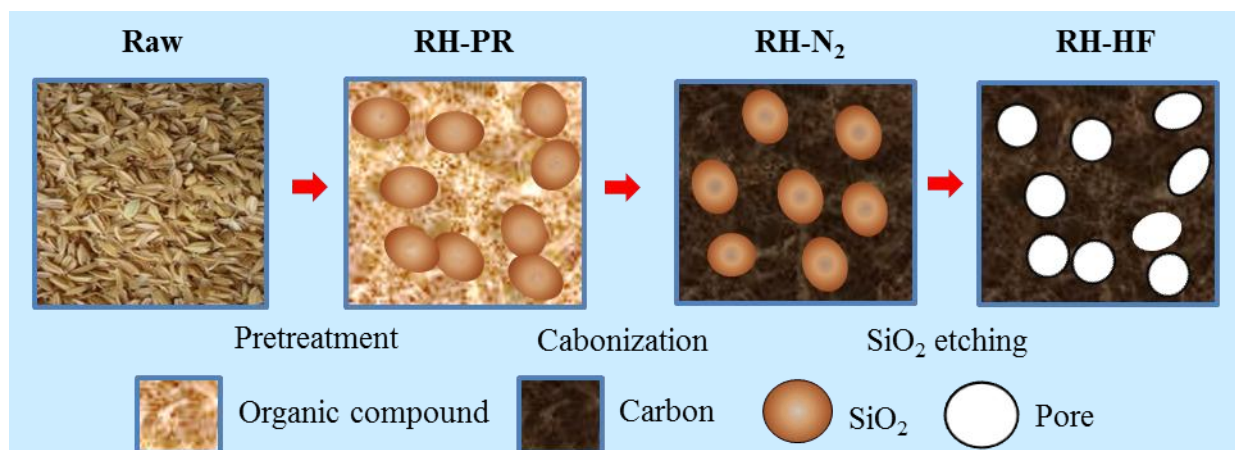


Figure 4. Model of porous carbon from rice husk.

RHs usually contain organic compounds such as lignin, cellulose and hemicelluloses, and other inorganic compounds such as K-, Na-, Mg-, and Si-compounds[11,12]. During the pretreatment of raw-RH at 260°C, organic and volatile compounds were decomposed or removed (RH-PR), and by carbonization of RH in inert atmosphere at 700°C, carbon and SiO₂ are remain (RH-N₂). When the inorganic compounds in RH-N₂ are removed by etching with HF solution, the mesopores are developed in RH-HF carbon by removal of inorganic compounds.

Table 1. Residual mass according to a TG analysis and the structural properties of carbon samples by BET plots and the BJH method.

Samples	TG	BET		BJH
	R_{mass}^a (wt%)	S_{BET}^b (m ² /g)	V_{total}^c (cm ³ /g)	V_{meso}^d (cm ³ /g)
Raw	9	1.63	0.01	0.01
RH-PR	22	58.77	0.04	0.01
RH-N ₂	29.2	292.63	0.15	0.02
RH-HF	3.79	398.31	0.26	0.13

^a Residual mass by TG analysis

^b BET surface area

^c Total pore volume

^d Micropore volume

Also, it is possible to calculate the specific surface area and pore area by BET and BJH plots using the nitrogen adsorption-desorption curve. The specific surface areas, the total pore area, and the

mesopores in the RH-N₂ and the RH-HF samples show that the amounts of adsorption and desorption increased. Particularly in the case of the mesopore area, as increase of nearly six times was noted after the removal of silica. The residual amount of inorganic components after the heat treatment was confirmed by the TG analysis. For RH-HF, it was possible to confirm a 26 wt% weight loss from the previous HF treatment. Moreover, it is expected that nearly 26 wt% of the silica and impurities were removed. However, a residual amount of 3.79 wt% of silica is likely isolated in the carbon structure [21]. The detailed values are given in Table 1.

3.2 Characterization of the PtRu/C catalyst

The PtRu/RH-N₂, PtRu/RH-HF and PtRu/XC-72R were processed using RH-N₂, RH-HF and commercial carbon black (XC-72R), respectively. A pH of 9 was set for the catalyst with aqueous ammonia (3 M) to handle the size of the Pt particles for producing the catalysts [22].

The platinum crystal phase appears to be very high in their XRD patterns. The peaks of both elements are scarcely observed. In addition, the XRD-patterns of the PtRu alloy for the fcc surface of [111], [200], [220], [311] appears in approximately $2\theta = 40^\circ, 46^\circ, 68^\circ$ and 81° , respectively [23]. This is also shown in the PtRu/RH-N₂, PtRu/RH-HF, and PtRu/XC-72R samples, suggesting that Pt and Ru are supported in all of the samples used in the experiment.

Table 2. Pt particle size, ECSA and on-set potential of the PtRu/XC-72R, PtRu/RH-N₂, and PtRu/RH-HF catalysts.

Catalysts	Catalyst	CO Stripping		Cyclic Voltammetry
	Pt particle size (nm)	ECSA _{co} (m ² /g-metal)	ECSA _{H₂} (m ² /g-metal)	On set Potential (V)
PtRu/XC-72R	1.75	31.37	21.18	2.68
PtRu/RH-N ₂	1.91	22.57	20.29	2.53
PtRu/RH-HF	2.98	47.97	53.58	2.44

The Pt crystal size was then calculated at the Pt (220) peak in the XRD pattern using the Scherrer equation (1) [24]. This value is shown in Table 2.

$$L = \frac{0.9\lambda_{\text{CuK}\alpha}}{B_{2\theta} \cos \theta_{\text{max}}} \quad (1)$$

Here, L is the size of the crystal, λ is the wavelength of the X-ray, θ is the Bragg angle and B denotes the radians. The Pt particle sizes of the PtRu/XC-72R, PtRu/RH-N₂ and PtRu/RH-HF samples were 1.75, 1.91 and 2.98 nm, respectively.

The FE-TEM images of the PtRu/RH-N₂ (a) and PtRu/RH-HF (b) catalysts with RH-N₂ and the RH-HF carbon supports, respectively, are shown in Fig. 5.

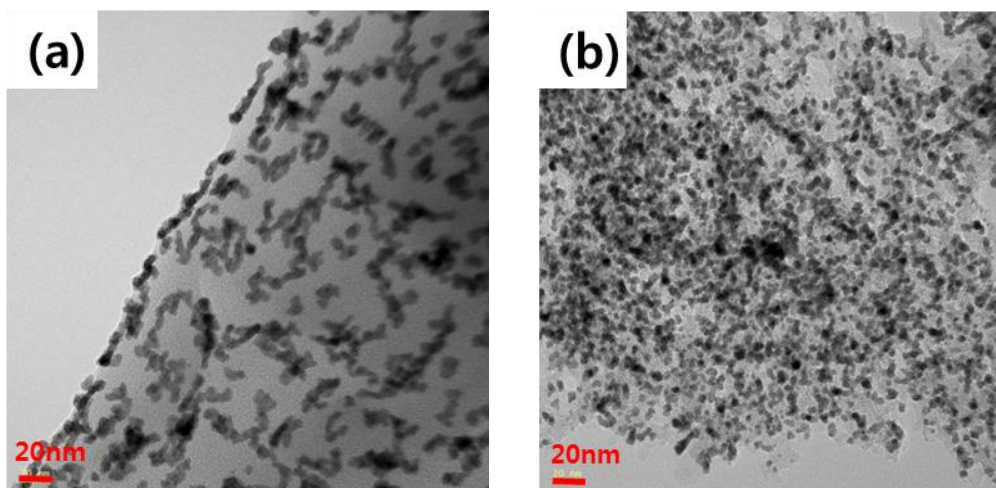


Figure 5. FE-TEM images of the PtRu/RH-N₂ (a) and PtRu/RH-HF (b) catalysts.

TEM images prove the PtRu nanoparticles (dark dots) are uniformly dispersed on carbon support (gray particles). The elongated and connected catalyst particles in the PtRu/RH-HF catalysts (Fig. 5(a)) are observed. When the PtRu particles supported on the RH-HF carbon supports the PtRu particles become more homogeneous and separated in shape as denoted by the overview TEM images (Fig. 5(b)). Due to the porous structure (pore diameter of 2~35 nm) (Fig. 3) and high BET surface area ($398.31 \text{ m}^2 \text{ g}^{-1}$) (Table 2) of RH-HF carbon, which was etched by a HF solution, the PtRu particles on the RH-HF carbon (PtRu/RH-HF catalysts) are more homogeneous distributed than that on the RH-N₂ carbon, as shown in Fig. 5(b). The average size of the PtRu nanoparticles measured from the overview images (ca. 2-3 nm) is in good agreement with the XRD data.

3.3 Electrochemical analysis of PtRu/C catalyst

The catalytic reaction is an immediate surface reaction. For this reason, the surface and/or the specific surface area are among the critical factors for a catalyst material. Therefore, a pre-investigation is necessary before measuring the catalytic activity of the electrode catalyst. Cyclic voltammograms (CV) were measured to determine the electrochemical surface areas (ECSAs) of the catalysts. Fig. 5 shows the CV results for PtRu/RH-N₂, PtRu/RH-HF, and PtRu/XC-72R with a sweep rate of 20 mV s^{-1} in $0.5 \text{ M H}_2\text{SO}_4$ solution. The CV curves show several types of forms along the crystal plane of Pt [25]. Several repeated peaks [26] appear, with processing done with polycrystalline platinum as a catalyst sample. The PtRu/RH-N₂, PtRu/RH-HF and PtRu/XC-72R samples have polycrystalline planes of Pt. These can be seen in the analysis results of the X-ray diffraction patterns. The curves of PtRu/XC-72R and PtRu/RH-N₂ are similar to the I-V behavior of the polycrystalline platinum catalyst from 0 to 0.2 V, as shown in Fig. 6. In contrast, the I-V behavior of PtRu/RH-HF has a different shape. Specifically, a steep peak from 0 to 0.05 V was noted in PtRu/RH-HF sample. It appears in the form of an inflection point in the graph.

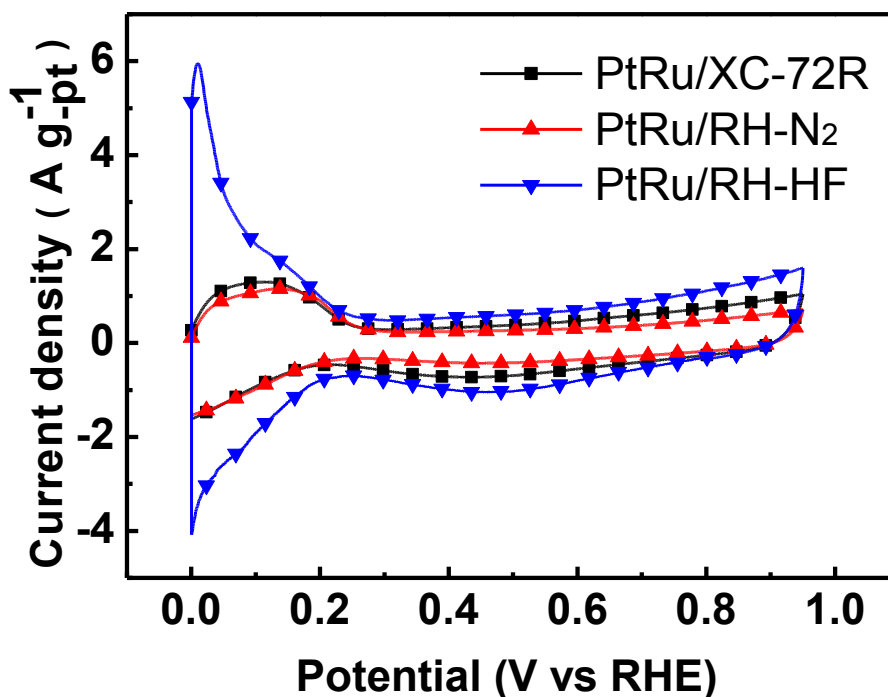


Figure 6. Cyclic voltammogram curves of the PtRu/XC-72R, PtRu/RH-N₂, and PtRu/RH-HF catalysts in a 0.5 M H₂SO₄ solution at 30 °C at a scan rate of 20 mV/s.

During the cathodic sweep at 0.0 ~ 0.2 V for the hydrogen adsorption reaction, the potential section shows as result of ($H^+ \rightarrow H_{ads}$), contrary to the anodic sweep at an interval of about 0.2 ~ 0.0 V to determine the amounts of adsorption and desorption. The ECSA_{H₂} values were measured by the hydrogen adsorption reaction ($H_{ads} \rightarrow H^+$). An electric double-layer region typically starts from approximately 0.2 V. With the charge quantity $Q_{H_2-adsorption}$ or $Q_{H_2-desorption}$, the ECSA_{H₂} can be calculated in both sections with the following equation (2) [27].

$$ECSA_{H_2} = \frac{Q_{H_2 \text{ ads or des (mC)}}}{0.21 \text{ (mC/gPt)} \times Pt \text{ loading (g/cm}^2\text{)}} \quad (2)$$

Here, 0.21 (mC/gPt) is the hydrogen value for the charge amount at the time the monolayer was adsorbed on the platinum surface [28]. In addition, Pt loading ($g \text{ cm}^{-2}$) indicates the amount of platinum per unit area of the production electrode. In this study, it was applied to the ECSA_{H₂} calculation using the hydrogen adsorption charge amount. It was found that the surface area increases in the order of PtRu/RH-HF, PtRu/XC-72R and PtRu/RH-N₂. The ECSA_{H₂} value of PtRu/RH-HF is nearly twice as large as those of the other samples, and the PtRu/XC-72R and PtRu/RH-N₂ had similar ECSA_{H₂} values. Table 2 shows detailed information about these values.

ESCA_{CO} was calculated and analyzed by an anode stripping method [29]. Pt has a very high CO adsorption [30]. The CV method involved circulation of nearly five times while adsorbing the CO into the sample. Different behavior appeared in this case. A large peak between 0.4 ~ 0.8 V formed during the first round of the circulation. The results of the next circulation round were similar to the

CV results shown in Fig 6. A graph of this sample shows typical CO stripping I-V behavior, as illustrated in Fig. 7.

The actual surface area of Pt was determined by calculating the areas of the peaks and the desorption amount of CO. Between the first and second arc curve intersects and the end point, the peak area was calculated [31]. With the charge quantity $Q_{\text{CO-adsorption}}$ or $Q_{\text{CO-desorption}}$, the ECSA_{CO} can be calculated for both sections using the following equation (3) [31].

$$\text{ECSA}_{\text{CO}} = \frac{Q_{\text{CO ads or des (mC)}}}{0.42_{(\text{mC/gPt})} \times \text{Pt loading}_{(\text{g/cm}^2)}} \quad (3)$$

Here, 0.42 (mC/gPt) is the CO value of the amount of charge at the time the monolayer was adsorbed onto the platinum surface [32]. In addition, Pt loading (g cm^{-2}) indicates the amount of platinum per unit area of the production electrode. The charge amount of CO desorption was applied to the ECSA calculation. As a result, the order of the samples was identical to that for ECSA_{H_2} . The details of these values can also be found in Table 2.

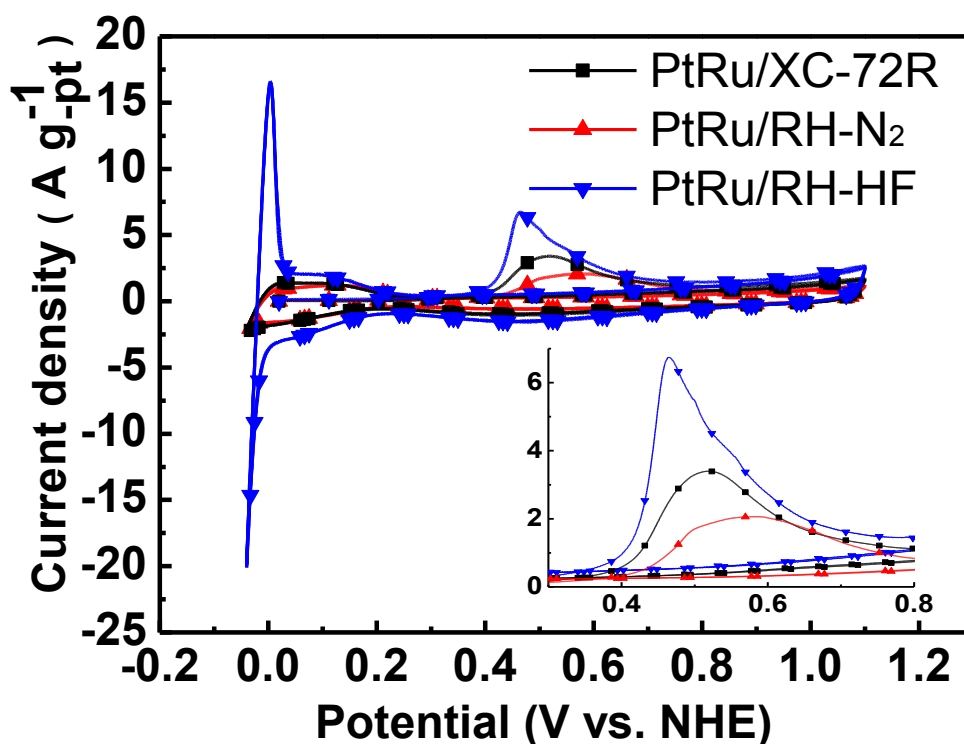


Figure 7. CO stripping voltammograms of the PtRu/XC-72R, PtRu/RH-N₂, and PtRu/RH-HF catalysts in a 0.5 M H₂SO₄ solution, at 30 °C at a scan rate of 20 mV/s.

Fig. 8 shows the CV of the methanol oxidization as recorded during the fifth circle under an acidic condition (0.5 M H₂SO₄ + 1.0 M CH₃OH). PtRu/RH-N₂, PtRu/RH-HF and PtRu/XC-72R catalysts show nearly identical methanol oxidization peak potentials of 0.46 V (vs. SCE). The peak current density of PtRu/XC-72R is clearly lower than those of the other samples. A low onset potential is important in methanol oxidization [33], as a low onset potential of a catalyst means a faster reaction

with methanol. The onset potential was calculated with a contact point of inclination ranging from 0.0 to 0.1 V and ranging from 0.3 to 0.4 V. In this regard, the value for PtRu/XC-72R is lower than those of the other catalysts. These values are shown in Table 2. This table shows the different behavior and values for ECSA_{H_2} and CO , indicating that the actual surface areas of the Pt and methanol oxidation reaction are not always consistent. However, this result has a significant impact on the performances of the two elements for DMFCs [34].

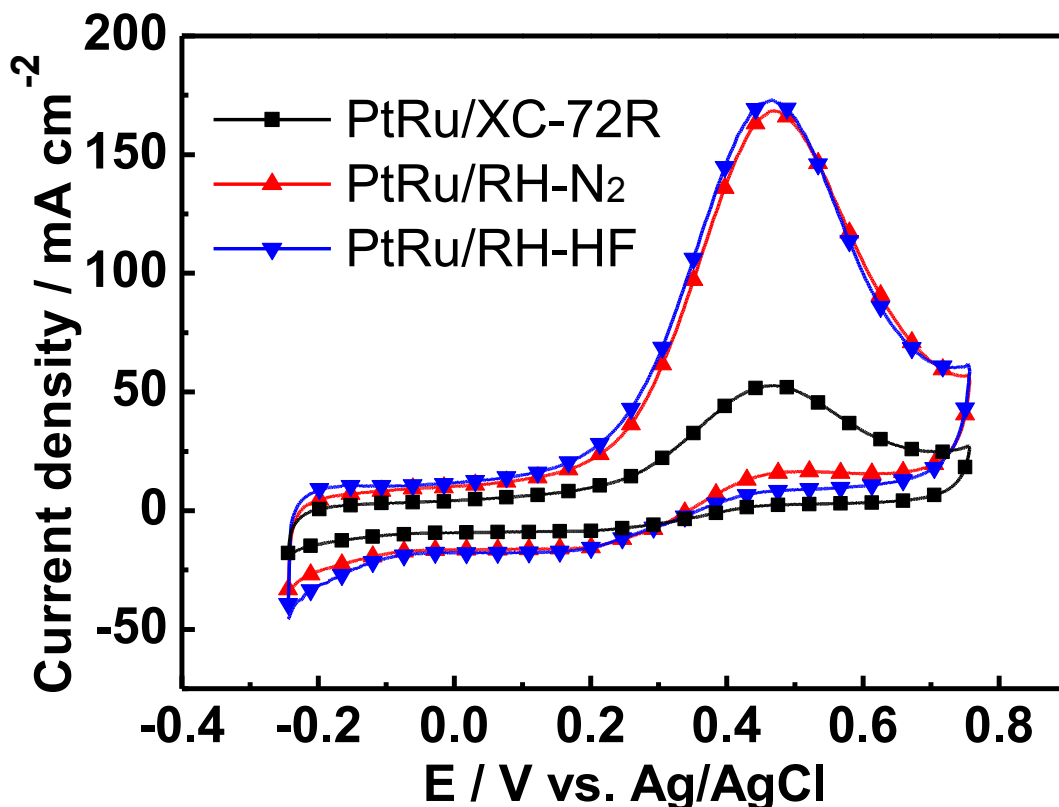


Figure 8. Cyclic voltammogram curves of the PtRu/XC-72R, PtRu/RH-N₂, and PtRu/RH-HF catalysts in a 0.5 M H₂SO₄ + 1.0 M CH₃OH solution at 30 °C at a scan rate of 50 mV/s.

A single-cell test was performed to evaluate the performance of MEA prepared with PtRu/XC-72R, PtRu/RH-N₂, PtRu/RH-HF, and PtRu/JM anode catalysts. The performance of MEA with PtRu/JM as the reference anode catalyst was also performed to compare the performance of MEAs with PtRu/XC-72R, PtRu/RH-N₂, PtRu/RH-HF, and PtRu/JM catalysts. PtRu/JM is a commercial catalyst with a 60 wt% PtRu metal content (JM10100, Johnson Matthey, UK). The MEA was kept wet for nearly 24 h and the cell performance were then evaluated under the constant current mode. At 60 °C, the single-cell performances (I-V curves) of MEAs using PtRu/XC-72R, PtRu/RH-N₂, PtRu/RH-HF and PtRu/JM are shown in Fig. 9.

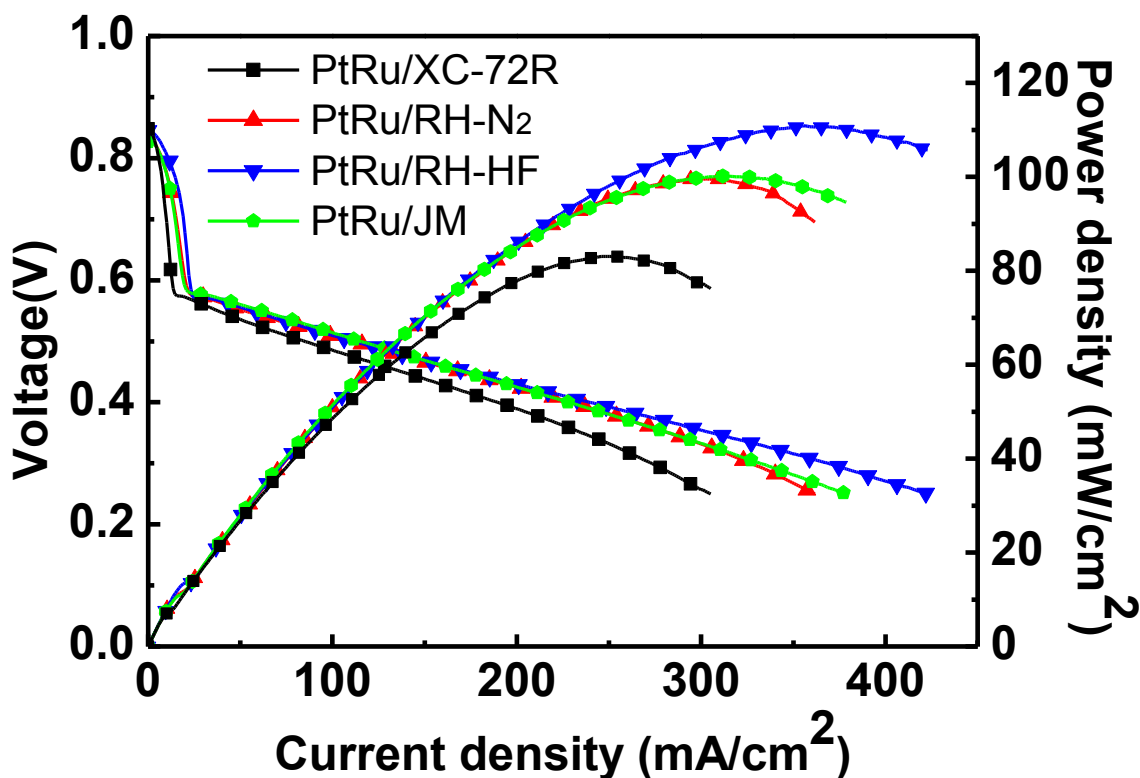


Figure 9. I-V and power density curves of PtRu/XC-72R, PtRu/RH-N₂, PtRu/RH-HF, and PtRu/JM at 60°C.

Under low and middle ranges of current densities (from 0 to 200 mA cm⁻²), the performances of the MEAs with PtRu/RH-N₂ and PtRu/RH-HF as anode catalysts are similar to that of PtRu/JM. However, when the current density reaches 250mA cm⁻², the fuel cell with PtRu/RH-HF catalyst performs better.

The rated and peak power densities of MEAs with the PtRu/XC-72R, PtRu/RH-N₂, and PtRu/RH-HF catalysts are shown in Table 3.

Table 3. Rated and peak power densities of MEAs with the PtRu/XC-72R, PtRu/RH-N₂, and PtRu/RH-HF catalysts.

Catalysts	Power densities (mW cm ⁻²)	
	at rated voltage (0.4 V)	at peak power
PtRu/XC-72R	75	83
PtRu/RH-N ₂	91	99
PtRu/RH-HF	95	110
PtRu/JM	91	100

The MEA with PtRu/RH-HF catalyst has the best performance at peak power and rated voltage (0.4V) due to the highest ECSA and lowest on-set potential of catalyst as shown in table 2.

4. CONCLUSION

Porous carbon as catalyst support was produced from RH for DMFCs. RH has excellent benefits because it has high silica content for a useful pore structure. Two types of catalyst supporters (RH-N₂ and RH-HF) were applied utilizing those properties. The carbonized sample RH-N₂ (292 m² g⁻¹) and the silica-etched sample RH-HF (398.31 m² g⁻¹) have a higher specific surface area than the commercial carbon black (XC-72R, 250 m² g⁻¹). In addition, they have high amounts of mesopores, which has an impact on the catalytic performance. The PtRu/C catalysts for DMFCs were first produced using RH-N₂ and RH-HF. The sizes of the Pt particles in the anode catalysts were approximately 1~3 nm.

In addition, CV and CO stripping methods were used to determine the electrochemical properties of the catalysts. ECSA_{H₂} and ECSA_{CO} were calculated. The PtRu/RH-HF sample shows the highest values among the samples. The performance abilities were determined by methanol oxidization of this sample by CV with an order of PtRu/RH-HF, PtRu/RH-N₂, and PtRu/XC-72R.

The catalyst was applied to a DMFC. The single-cell test result is similar to the ECSA and methanol oxidization results. PtRu/RH-HF catalyst shows higher performance than the commercial catalyst (JM10100). The maximum (at 0.3 V) and rated (at 0.4 V) power densities of MEA with PtRu/RH-HF were 110 and 95 mW cm⁻², respectively, at 60 °C. These power densities were increased by 32 and 26 %, respectively, than that of PtRu/XC-72R. Porous carbon (RH-HF and RH-N₂) from RH as a catalyst support showed higher performance than the commercial carbon black (XC-72R).

ACKNOWLEDGEMENTS

This work was supported by the New & Renewable Energy R&D Program (2012T100201695) of the Korea Institute of Energy Technology Evaluation and Planning (KETEP), granted financial resource from the Ministry of Trade, Industry & Energy, Republic of Korea.

References

1. H. Liu, C. Song, L. Zhang, J. Zhang, H. Wang, D.P. Wilkinson, *J. Power Sources*, 155 (2006) 95
2. R.N. Singh, R. Awasthi, C.S. Sharma, *Int. J. Electrochem. Sci.*, 9 (2014) 5607
3. R. Ramachandran, G.P.G. Kumar, S.M. Chen, *Int. J. Electrochem. Sci.* 11 (2016) 506
4. S. Jingyu, H. Jianshu, C. Yanxia, Z. Xiaogang, *Int. J. Electrochem. Sci.* 2 (2007) 64
5. K.D. Nam, S.Y. Lim, S.K. Kim, D.H. Peck, D.H. Jung, *J. Nanoscience and Nanotechnology* , 11 (2011) 5761
6. X. Wang, W. Li, Z. Chen, M. Waje, Y. Yan, *J. Power Sources*, 158 (2006) 154
7. J.S. Jang, S.Y. Lim, S.K. Kim, D.H. Peck, B.R. Lee, C.M. Yoon, D.H. Jung, *J. Nanoscience and Nanotechnology* , 11 (2011) 5775
8. Y.I. Kim, D. Soundararajan, C.W. Park, S.H. Kim, J.H. Park, J.M. Ko, *Int. J. Electrochem. Sci.* 4 (2009) 1548

9. K.D. Nam, S.Y. Lim, S.K. Kim, S.H. Yoon, D.H. Jung, *International J. Hydrogen Energy*, 37 (2012) 4619
10. N. Soltani, A. Bahrami, M.I. Pech-Canul, L.A. Gonzalez, *Chemical Engineering Journal*, 264 (2015) 899
11. S. Kumagai, J. Sasaki, *Bioresource technology*, 100 (2009) 3308
12. M. Rozainee, S.P. Ngo, A.A. Salema, K.G. Tan, M. Ariffin, Z.N. Zainura, *Bioresource Technology*, 99 (2008) 703
13. Y. Gao, L. Li, Y. Jin, Y. Wang, C. Yuan, Y. Wei, G. Chen, J. Ge, H. Lu, *Applied Energy*, 153 (2015) 41
14. Y. Guo, D.A. Rockstraw, *Microporous and Mesoporous Materials*, 100 (2007) 12
15. E.Y.L. Teo, L. Muniandy, E.P. Ng, F. Adam, A.R. Mohamed, R. Jose, K.F. Chong, *Electrochimica Acta*, 192 (2016) 110
16. C.H. Yun, Y.H. Park, C.R. Park, *Carbon*, 39 (2001) 559-567
17. Y. Ju, J.A. Tang, K. Zhu, Y. Meng, C. Wang, G. Chen, Y. Wei, Y. Gao, *Electrochimica Acta*, 191 (2016) 411
18. L. Wang, Z. Schnepf, M.M. Titirici, *J. Materials Chemistry. A*, 1 (2013) 5269
19. R. Khan, A. Jabbar, I. Ahmad, W. Khan, A.N. Khan, J. Mirza, *Construction and Building Materials*, 30 (2012) 360
20. M.S. Hyun, S.K. Kim, B.R. Lee, D.H. Peck, Y.G. Shul, D.H. Jung, *Catalysis Today*, 132 (2008) 138
21. R.V. Krishnarao, M.M. Godkhindi, *Ceramics International*, 18 (1992) 243
22. K.D. Nam, University of Science and Technology (UST), Korea, PhD thesis (2012)
23. E. Antolini, F. Cardellini, *J. Alloys and Compounds*, 315 (2001) 118
24. A. Monshi, M.R. Foroughi, M.R. Monshi, *World J. Nano Science and Engineering*, 2 (2012) 154
25. T.J. Schmidt, H.A. Gasteiger, G.D. Stäb, P.M. Urban, D.M. Kolb, R.J. Behm, *J. Electrochem. Soc.*, 145 (1998) 2354
26. W.K. Paik, S.M. Park, *Electrochemistry: Science and technology of electrode processes*, Seoul, Cheong Moon Gak (2001).
27. G. Girishkumar, M. Rettker, R. Underhille, D. Binz, K. Vinodgopal, P. Mcginn, P. Kamatl, *Langmuir*, 21 (2005) 8487
28. W. Vielstich, H. Gasteiger, A. Lamm, *Handbook of fuel cells Fundamental. Technology and Applications*, West Sussex, Wiley (2003)
29. A.R. Corpuz, T.S. Olson, P. Joghee, S. Pylypenko, A.A. Dammeron, H.N. Dinh, K.J. O'Neill, K.E. Hurst, G. Bender, T. Gennett, B.S. Pivovar, R.M. Richards, R.P. O'Hayre, *J. Power Sources*, 217 (2012) 142
30. S.H. Park, S.J. Joo, H.S. Kim, *J. Electrochem. Soc.*, 161 (2014) F405
31. T. Vidaković, M. Christov, K. Sundmacher, *Electrochimica Acta*, 52 (2007) 5606
32. F. Maillard, S. Schreier, M. Hanzlik, E.R. Savinova, S. Weinkauff, U. Stimming, *Phys. Chem. Chem. Phys.*, 7 (2005) 385
33. I.S. Park, K.W. Park, J.H. Choi, C.R. Park, Y.E. Sung, *Carbon*, 45 (2007) 28
34. J.H. Choi, K.J. Jeong, Y.J. Dong, J.H. Han, T.H. Lim, J.S. Lee, Y.E. Sung, *J. Power Sources*, 163 (2006) 71